MOLECULAR AND CELLULAR BIOLOGY, Oct. 2009, p. 5552–5563 Vol. 29, No. 20
0270-7306/09/$08.00+0 doi:10.1128/MCB.00476-09

Cell Cycle-Dependent Role of MRN at Dysfunctional Telomeres: ATM Signaling-Dependent Induction of Nonhomologous End Joining (NHEJ) in G_1 and Resection-Mediated Inhibition of NHEJ in G_2 ▽†

Nadya Dimitrova‡ and Titia de Lange*

The Rockefeller University, 1230 York Avenue, New York, New York 10065

Received 13 April 2009/Returned for modification 26 May 2009/Accepted 30 July 2009

Here, we address the role of the MRN (Mre11/Rad50/Nbs1) complex in the response to telomeres rendered dysfunctional by deletion of the shelterin component TRF2. Using conditional NBS1/TRF2 double-knockout MEFs, we show that MRN is required for ATM signaling in response to telomere dysfunction. This establishes that MRN is the only sensor for the ATM kinase and suggests that TRF2 might block ATM signaling by interfering with MRN binding to the telomere terminus, possibly by sequestering the telomere end in the t-loop structure. We also examined the role of the MRN/ATM pathway in nonhomologous end joining (NHEJ) of damaged telomeres. NBS1 deficiency abrogated the telomere fusions that occur in G_1, consistent with the requirement for ATM and its target 53BP1 in this setting. Interestingly, NBS1 and ATM, but not H2AX, repressed NHEJ at dysfunctional telomeres in G_2, specifically at telomeres generated by leading-strand DNA synthesis. Leading-strand telomere ends were not prone to fuse in the absence of either TRF2 or MRN/ATM, indicating redundancy in their protection. We propose that MRN represses NHEJ by promoting the generation of a 3′ overhang after completion of leading-strand DNA synthesis. TRF2 may ensure overhang formation by recruiting MRN (and other nucleases) to newly generated telomere ends. The activation of the MRN/ATM pathway by the dysfunctional telomeres is proposed to induce resection that protects the leading-strand ends from NHEJ when TRF2 is absent. Thus, the role of MRN at dysfunctional telomeres is multifaceted, involving both repression of NHEJ in G_2 through end resection and induction of NHEJ in G_1 through ATM-dependent signaling.

Mammalian telomeres solve the end protection problem through their association with shelterin. The shelterin factor TRF2 (telomere repeat-binding factor 2) protects chromosome ends from inappropriate DNA repair events that threaten the integrity of the genome (reviewed in reference 32). When TRF2 is removed by Cre-mediated deletion from conditional knockout mouse embryo fibroblasts ($TRF2^{F/-}$ MEFs), telomeres activate the ATM kinase pathway and are processed by the canonical nonhomologous end-joining (NHEJ) pathway to generate chromosome end-to-end fusions (10, 11).

The repair of telomeres in TRF2-deficient cells is readily monitored in metaphase spreads. Over the course of four or five cell divisions, the majority of chromosome ends become fused, resulting in metaphase spreads displaying the typical pattern of long trains of joined chromosomes (10). The reproducible pace and the efficiency of telomere NHEJ have allowed the study of factors involved in its execution and regulation. In addition to depending on the NHEJ factors Ku70 and DNA ligase IV (10, 11), telomere fusions are facilitated by the ATM kinase (26). This aspect of telomere NHEJ is mediated through the ATM kinase target 53BP1. 53BP1 accumulates at telomeres in TRF2-depleted cells and stimulates chromatin mobility, thereby promoting the juxtaposition of distantly positioned chromosome ends prior to their fusion (18). Telomere NHEJ is also accelerated by the ATM phosphorylation target MDC1, which is required for the prolonged association of 53BP1 at sites of DNA damage (19).

Although loss of TRF2 leads to telomere deprotection at all stages of the cell cycle, NHEJ of uncapped telomeres takes place primarily before their replication in G_1 (25). Postreplicative (G_2) telomere fusions can occur at a low frequency upon TRF2 deletion, but only when cyclin-dependent kinase activity is inhibited with roscovitine (25). The target of Cdk1 in this setting is not known.

Here, we dissect the role of the MRN (Mre11/Rad50/Nbs1) complex and H2AX at telomeres rendered dysfunctional through deletion of TRF2. The highly conserved MRN complex has been proposed to function as the double-stranded break (DSB) sensor in the ATM pathway (reviewed in references 34 and 35). In support of this model, Mre11 interacts directly with DNA ends via two carboxy-terminal DNA binding domains (13, 14); the recruitment of MRN to sites of damage is independent of ATM signaling, as it occurs in the presence of the phosphoinositide-3-kinase-related protein kinase inhibitor caffeine (29, 44); in vitro analysis has demonstrated that MRN is required for activation of ATM by linear DNAs (27); a mutant form of Rad50 (Rad50S) can induce ATM signaling in the absence of DNA damage (31); and phosphorylation of

* Corresponding author. Mailing address: Laboratory for Cell Biology and Genetics, The Rockefeller University, 1230 York Avenue, New York, NY 10065-6399. Phone: (212) 327-8146. Fax: (212) 327-7147. E-mail: delange@mail.rockefeller.edu.

† Supplemental material for this article may be found at http://mcb.asm.org/.

‡ Present address: The David H. Koch Institute for Integrative Cancer Research at MIT, 40 Ames Street, Cambridge, MA 02142.

▽ Published ahead of print on 10 August 2009.

ATM targets in response to ionizing radiation is completely abrogated upon deletion of NBS1 from MEFs (17). These data and the striking similarities between syndromes caused by mutations in ATM, Nbs1, and Mre11 (ataxia telangiectasia, Nijmegen breakage syndrome, and ataxia telangiectasia-like disease, respectively) are consistent with a sensor function for MRN.

MRN has also been implicated in several aspects of DNA repair. Potentially relevant to DNA repair events, Mre11 dimers can bridge and align the two DNA ends in vitro (49) and Rad50 may promote long-range tethering of sister chromatids (24, 50). In addition, a binding partner of the MRN complex, CtIP, has been implicated in end resection of DNA ends during homology-directed repair (39, 45). The role of MRN in NHEJ has been much less clear. MRX, the yeast orthologue of MRN, functions during NHEJ in *Saccharomyces cerevisiae* but not in *Schizosaccharomyces pombe* (28, 30). In mammalian cells, MRN is not recruited to I-SceI-induced DSBs in G_1, whereas Ku70 is, and MRN does not appear to be required for NHEJ-mediated repair of these DSBs (38, 54). On the other hand, MRN promotes class switch recombination (37) and has been implicated in accurate NHEJ repair during V(D)J recombination (22).

The involvement of MRN in ATM signaling and DNA repair pathways has been intriguing from the perspective of telomere biology. While several of the attributes of MRN might be considered a threat to telomere integrity, MRN is known to associate with mammalian telomeres, most likely through an interaction with the TRF2 complex (48, 51, 57). MRN has been implicated in the generation of the telomeric overhang (12), the telomerase pathway (36, 52), the ALT pathway (55), and the protection of telomeres from stochastic deletion events (1). It has also been speculated that MRN may contribute to formation of the t-loop structure (16). t-loops, the lariats formed through the strand invasion of the telomere terminus into the duplex telomeric DNA (21), are thought to contribute to telomere protection by effectively shielding the chromosome end from DNA damage response factors that interact with DNA ends, including nucleases, and the Ku heterodimer (15).

H2AX has been studied extensively in the context of chromosome-internal DSBs. When a DSB is formed, ATM acts near the lesion to phosphorylate a conserved carboxy-terminal serine of H2AX, a histone variant present throughout the genome (7). Phosphorylated H2AX (referred to as γ-H2AX) promotes the spreading of DNA damage factors over several megabases along the damaged chromatin and mediates the amplification of the DNA damage signal (43). The signal amplification is accomplished through a sequence of phospho-specific interactions among γ-H2AX, MDC1, NBS1, RNF8, and RNF168, which results in the additional binding of ATM and additional phosphorylation of H2AX in adjacent chromatin (reviewed in reference 33). The formation of these large domains of altered chromatin, referred to as irradiation-induced foci at DSBs and telomere dysfunction-induced foci (TIFs) at dysfunctional telomeres (44), promotes the binding of several factors implicated in DNA repair, including the BRCA1 A complex and 53BP1 (33).

In agreement with a role for H2AX in DNA repair, H2AX-deficient cells exhibit elevated levels of irradiation-induced chromosome abnormalities (5, 9). In addition, H2AX-null B cells are prone to chromosome breaks and translocations in the immunoglobulin locus, indicative of impaired class switch recombination, a process that involves the repair of DSBs through the NHEJ pathway (9, 20). Since H2AX is dispensable for the activation of irradiation-induced checkpoints (8), these data argue that H2AX contributes directly to DNA repair. However, a different set of studies has concluded that H2AX is not required for NHEJ during V(D)J recombination (5, 9) but that it plays a role in homology-directed repair (53). In this study, we have further queried the contribution of H2AX to NHEJ in the context of dysfunctional telomeres.

Our aim was to dissect the contribution of MRN and H2AX to DNA damage signaling and NHEJ-mediated repair in response to telomere dysfunction elicited by deletion of TRF2. Importantly, since ATM is the only kinase activated in this setting, deletion of TRF2 can illuminate the specific contribution of these factors in the absence of the confounding effects of ATR signaling (26). This approach revealed a dual role for MRN at telomeres, involving both its function as a sensor in the ATM pathway and its ability to protect telomeres from NHEJ under certain circumstances.

MATERIALS AND METHODS

Generation of MEFs and deletion of conditional alleles. MEFs from E13.5 embryos obtained from crosses between $TRF2^{F/F}$ and $NBS1^{F/-}$, $TRF2^{F/F}$ and $H2AX^{+/-}$, and $TRF2^{F/-}$ $ATM^{-/-}$ and $Lig4^{-/-}$ mice (E. Lazzerini Denchi and T. de Lange, unpublished data) were isolated and immortalized at passage 2 with pBabeSV40LT (a gift from G. Hannon). Simian virus 40 (SV40)-transformed $TRF2^{F/-}$ $ATM^{+/-}$ and $TRF2^{F/-}$ $ATM^{-/-}$ were previously described (26). To delete TRF2 or NBS1, Cre was introduced by retroviral infection using the pMMP Hit&Run Cre retroviral construct (40). Briefly, Hit&Run Cre was expressed in ecotropic Phoenix cells. Virus-containing supernatant was collected at 36, 48, and 60 h posttransfection, and MEFs were infected consecutively three times every 12 h. The medium was changed 12 h after the last infection, and cells were analyzed at the indicated time points after the second infection.

Immunoblotting. Cells were lysed in 2× Laemmli buffer (100 mM Tris-HCl, pH 6.8, 200 mM dithiothreitol, 3% sodium dodecyl sulfate, 20% glycerol, 0.05% bromophenol blue) at 10^4 cell per μl, denatured for 7 min at 100°C, and sheared with an insulin needle before the equivalent of 2×10^5 cells per lane was loaded. After immunoblot analysis, membranes were blocked in phosphate-buffered saline (PBS) with 5% milk and 0.1% Tween and incubated with the following primary antibodies in 5% milk and 0.1% Tween: H2AX (rabbit polyclonal; 11175; Abcam), NBS1 (rabbit polyclonal; a gift from J. Petrini), TRF2 (rabbit polyclonal; 1254 [10]), Chk2 (mouse monoclonal; BD Biosciences), ATM-S1981-P (mouse monoclonal; Cell Signaling), and ATM (MAT3; Sigma). γ-Tubulin (clone GTU 488; Sigma) was used as a loading control. Blots were developed with enhanced chemiluminescence (Amersham).

Immunofluorescence-fluorescence in situ hybridization (FISH). Cells were grown on coverslips and fixed for 10 min in 2% paraformaldehyde at room temperature (RT) (γ-H2AX, MDC1, and 53BP1), followed by PBS washes, or the cells were fixed for 10 min in 1:1 methanol-acetone at −20°C (NBS1), followed by dehydration and rehydration in PBS for 5 min. Coverslips were blocked for 30 min in blocking solution (1 mg/ml bovine serum albumin, 3% goat serum, 0.1% Triton X-100, 1 mM EDTA in PBS). Next, the cells were incubated with the following primary antibodies diluted in blocking solution for 1 h at RT: 53BP1 (rabbit polyclonal; 100-304A; Novus Biologicals), γ-H2AX-S139-P (mouse monoclonal; Upstate Biotechnology), MDC1 (mouse monoclonal; a gift from J. Chen), and NBS1 (rabbit polyclonal; a gift from J. Petrini). After PBS washes, coverslips were incubated with rhodamine Red-X-labeled secondary antibody raised against mouse or rabbit (RRX; Jackson) for 30 min and washed in PBS. At this point, coverslips were fixed with 2% paraformaldehyde for 10 min at RT; washed extensively in PBS; dehydrated consecutively in 70%, 90%, and 100% ethanol for 5 min each; and allowed to dry completely. Hybridization solution (70% formamide, 1 mg/ml blocking reagent [Roche], 10 mM Tris-HCl, pH 7.2), containing the peptide nucleic acid (PNA) probe fluorescein isothiocyanate (FITC)-OO-$(CCCTAA)_3$ (Applied Biosystems), was added to each coverslip, and the cells were denatured by heating for 10 min at 80°C on a heat block.

After a 2-h incubation at RT in the dark, cells were washed twice with washing solution (70% formamide, 10 mM Tris-HCl, pH 7.2) and twice in PBS. DNA was counterstained with DAPI (4′,6-diamidino-2-phenylindole) and slides were mounted in antifade reagent (ProLong Gold; Invitrogen). Digital images were captured with a Zeiss Axioplan II microscope with a Hamamatsu C4742-95 camera, using Improvision OpenLab software.

Telomere FISH. At the indicated time points after Cre infection, cells were incubated for 1 h and 15 min with 0.2 μg/ml colcemid, harvested by trypsinization, swollen in KCl, and fixed overnight in methanol-acetic acid (3:1). When indicated, cells were treated for 4 h prior to being harvested with 50 μM roscovitine. The following day, metaphases were dropped on glass slides in a controlled environment (thermocycler; 20°C; 50% humidity) and aged overnight. For PNA FISH, slides were washed in PBS once and fixed in 4% formaldehyde for 2 min at RT. After extensive PBS washes, spreads were digested for 10 min at 37°C with 1 mg/ml pepsin dissolved in 10 mM glycine, pH 2.2. Slides were then washed in PBS, fixed again in 4% formaldehyde for 2 min at RT, and washed in PBS before dehydration by consecutive 5-min incubations in 70%, 90%, and 100% ethanol. After air drying, hybridization solution containing the FITC-OO-$(CCCTAA)_3$ PNA probe (Applied Biosystems) was added and spreads were denatured by heating for 3 min at 80°C on a heat block. Spreads were then allowed to hybridize in the dark for 2 h at RT. Two 15-min washes were performed with washing solution 1 (70% formamide, 10 mM Tris-HCl, pH 7.0, 0.1% bovine serum albumin), followed by three washes in washing solution 2 (0.1 M Tris-HCl, pH 7.0, 0.15 M NaCl, 0.08% Tween 20), with DAPI added to the second wash to counterstain the chromosomal DNA. Slides were dehydrated in an ethanol series (75%, 90%, and 100%) and were mounted in antifade reagent (ProLong Gold; Invitrogen). Digital images were captured with a Zeiss Axioplan II microscope with a Hamamatsu C4742-95 camera, using Improvision OpenLab software.

Telomere chromosome orientation-FISH (CO-FISH). Cells were grown in the presence of 10 μM BrdU-BrdC (3:1) for 16 h, and colcemid was added for the last 1 h and 15 min at a concentration of 0.2 μg/ml. Metaphases were harvested, fixed, and spread on glass slides as described for FISH. Prior to hybridization, slides were washed once with PBS, treated with RNase A (0.5 mg/ml in PBS) for 10 min at 37°C, stained with Hoechst 33258 (0.5 mg/ml in 2× SSC [1× SSC is 0.15 M NaCl plus 0.015 M sodium citrate]) for 10 min at RT, and exposed to 365-nm UV light (Stratalinker 1800 UV irradiator) for 30 min. The BrdU-BrdC-substituted DNA strand was digested with exonuclease III (10 U/ml) for 10 min at RT. The slides were dehydrated in an ethanol series (75%, 90%, and 100%) and hybridized to the TAMRA (6-carboxytetramethylrhodamine)-OO-$(TTAGGG)_3$ PNA probe (Applied Biosystems) in hybridization solution (see FISH protocol) for 2 h in the dark at RT. Next, the slides were briefly washed in washing solution 1 (see FISH protocol) and incubated with the FITC-OO-$(CCCTAA)_3$ PNA probe (Applied Biosystems) in hybridization solution for 2 h in the dark at RT. The subsequent washing, mounting, and visualization steps were performed as for the FISH protocol.

In-gel analysis of telomeric DNA. Pulsed-field gel electrophoresis and in-gel detection of mouse telomeric DNA were done as described previously (46). Cells were resuspended in PBS and mixed 1:1 (vol/vol) with 2% agarose (SeaKem agarose) to obtain 5×10^5 cells per agarose plug. Plugs were digested overnight with 1 mg/ml proteinase K (in buffer containing 100 mM EDTA, 0.2% sodium deoxycholate, 1% sodium lauryl sarcosine), washed extensively with TE buffer (10 mM Tris-HCl, pH 8.0, 1 mM EDTA), and incubated overnight at 37°C with 60 U MboI. The following day, the plugs were washed once in TE and once in water and equilibrated in 0.5× Tris-borate-EDTA (TBE). Plugs were loaded on a 1% agarose-0.5× TBE gel and run for 24 h using a CHEF-DRII pulsed-field gel electrophoresis apparatus (Bio-Rad) in 0.5× TBE running buffer. The settings were as follows: initial pulse, 5 min; final pulse, 5 min; 6 V/cm^2; and 14°C. In-gel hybridization of the native gel with [γ-^{32}P]ATP end-labeled $(CCCTAA)_4$ oligonucleotides and subsequent denaturation and hybridization steps were performed as described previously (46). Gels were exposed on a PhosphorImager screen overnight, and a single-stranded G-overhang signal was quantified with ImageQuant software and normalized to the total telomeric DNA quantified after denaturation. The percents overhang value given represent the ratios of the overhang signal detectable at different time points (normalized to the total TTAGGG repeat signal in the same lane) in comparison to the overhang signal for the same cells not treated with Cre.

RESULTS

MRN as the only sensor in the ATM response to telomere dysfunction. To address the role of NBS1 in the ATM-mediated response to telomere damage elicited by loss of TRF2, we crossed NBS1$^{F/-}$ (37, 56) mice with TRF2$^{F/F}$ (10) mice. We isolated TRF2$^{F/F}$ NBS1$^{F/+}$ and TRF2$^{F/F}$ NBS1$^{F/-}$ MEFs from E13.5 littermate embryos and immortalized the cells at passage 2 with SV40 large T antigen, abrogating the p53 pathway. Efficient Cre-mediated deletion of NBS1 and TRF2 in the various MEF lines was confirmed by immunoblotting (Fig. 1A).

Depletion of TRF2 in control, NBS1-proficient MEFs led to activation of the ATM signaling pathway, evidenced by the presence of the autophosphorylated, active form of the ATM kinase, ATM-S1981-P, and by the extensive phosphorylation of the ATM kinase target, Chk2 (Fig. 1A) (11). Consistent with a requirement for MRN as the sensor in the ATM kinase pathway, both ATM autophosphorylation and Chk2 phosphorylation were abrogated when Nbs1 was absent (Fig. 1A). Furthermore, deletion of NBS1 eliminated the formation of discernible TIF containing γ-H2AX, MDC1, and 53BP1 (Fig. 1B). Quantification of Cre-treated TRF2$^{F/F}$ NBS1$^{F/+}$ and TRF2$^{F/F}$ NBS1$^{F/-}$ MEFs revealed that whereas 89% ± 2% of control cells had more than 10 53BP1 TIFs per cell, only ~1% of NBS1-deficient cells were TIF positive (Fig. 1C). The absence of checkpoint signaling and the abrogation of TIF in NBS1-deficient cells with telomere dysfunction recapitulate the phenotypes of ATM loss and substantiate the conclusion that the MRN complex is the only sensor in the ATM pathway.

For comparison, we examined the role of another chromatin-associated DNA damage response factor, H2AX, in the ATM-mediated response to telomere dysfunction. Similar to what was found for NBS1, deficiency in H2AX abolished the formation of cytologically discernible NBS1, MDC1, and 53BP1 TIFs in Cre-treated TRF2$^{F/F}$ H2AX$^{-/-}$ MEFs (see Fig. S1A in the supplemental material). Quantitative analysis revealed that less than 1% of the H2AX-deficient cells contained 10 or more 53BP1 foci at deprotected telomeres, compared to more than 90% of H2AX-proficient cells (see Fig. S1B in the supplemental material). The requirement for H2AX in TIF formation is consistent with its role in promoting irradiation-induced-focus formation. However, unlike for NBS1, deficiency in H2AX only diminished and did not abolish Chk2 phosphorylation (see Fig. S1C in the supplemental material). Altogether, these data draw a distinction between the sensor MRN complex, which is required for the activation of the ATM pathway, and other chromatin-associated DNA damage response factors, such as H2AX, which contribute to the amplification of the damage signal.

NBS1 promotes G_1 chromosome-type fusions. Next, we asked whether NBS1 played a role in the NHEJ pathway that processes dysfunctional telomeres upon loss of TRF2. We compared the frequencies of fused chromosome ends in metaphase chromosome spreads collected from TRF2$^{F/F}$ NBS1$^{F/+}$ and TRF2$^{F/F}$ NBS1$^{F/-}$ MEFs at successive time points after Cre-mediated deletion of TRF2. As expected, in control NBS1-proficient cells, we observed a progressive increase in the frequency of fused chromosome ends (Fig. 2). At 96 h after Cre treatment, 50% ± 10% of the chromosome ends had fused, and at 120 h, this frequency increased to 60% ± 2% (Fig. 2A and C). Deletion of TRF2 from NBS1-deficient cells also led to the occurrence of telomere fusions, but the frequencies were greatly reduced, to 4% ± 0.4% and 13% ± 3%, at 96

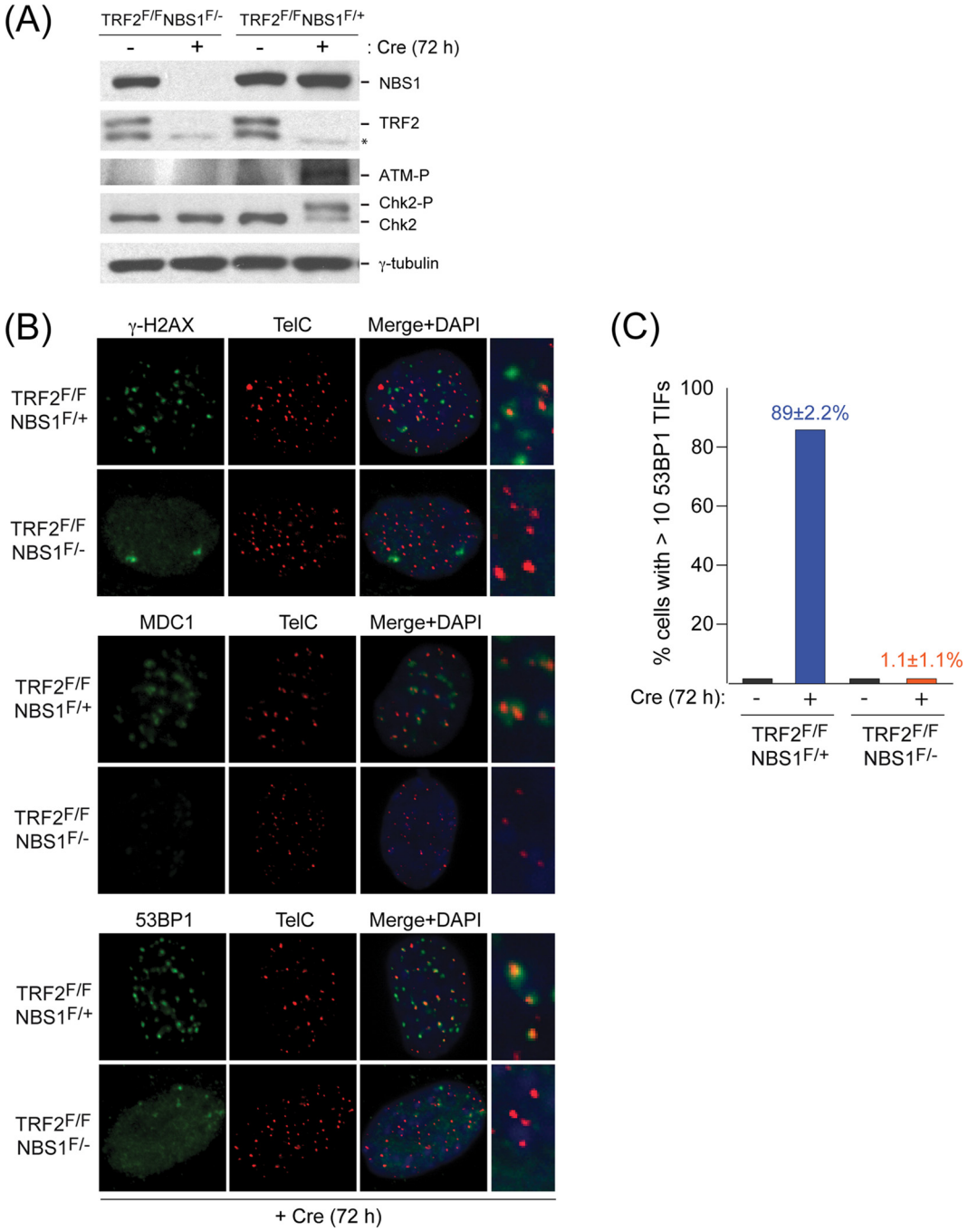

FIG. 1. The MRN complex is the sensor in the ATM pathway. (A) Immunoblots detecting NBS1, TRF2, ATM-S1981-P, and Chk2 phosphorylation in indicated MEFs, harvested untreated or 72 h after Cre infection. γ-Tubulin was used as a loading control. * indicates a nonspecific band. (B) Effects of NBS1 deletion on γ-H2AX, MDC1, and 53BP1 TIF formation. $TRF2^{F/F}$ $NBS1^{F/+}$ and $TRF2^{F/F}$ $NBS1^{F/-}$ MEFs, harvested 72 h after Cre treatment and processed for immunofluorescence-FISH (γ-H2AX, MDC1, or 53BP1 [green] costained with telomeric TTAGGG-specific FISH probe [red] or DAPI [blue]). Images were merged and enlarged. (C) Frequency of TIF-positive cells. At least 150 cells processed as described for panel B were scored for 10 or more telomeric 53BP1 foci. Average values and standard deviations for three independent experiments are indicated.

and 120 h after Cre treatment, respectively (Fig. 2A and C). The decreased rate of NHEJ was not due to changes in proliferation, since growth rates were comparable for Cre-treated NBS1-proficient and -deficient cells (see Fig. S2 in the supplemental material), arguing that NBS1 directly promotes the repair of dysfunctional telomeres.

Interestingly, in addition to the overall reduction in the frequency of telomere fusions in TRF2/NBS1-deficient cells, we noted a marked shift in the type of fusions. The repair of TRF2-depleted telomeres takes place primarily before DNA replication, presumably in G_1, leading to chromosome-type fusions in metaphase spreads (25). In accordance, we found

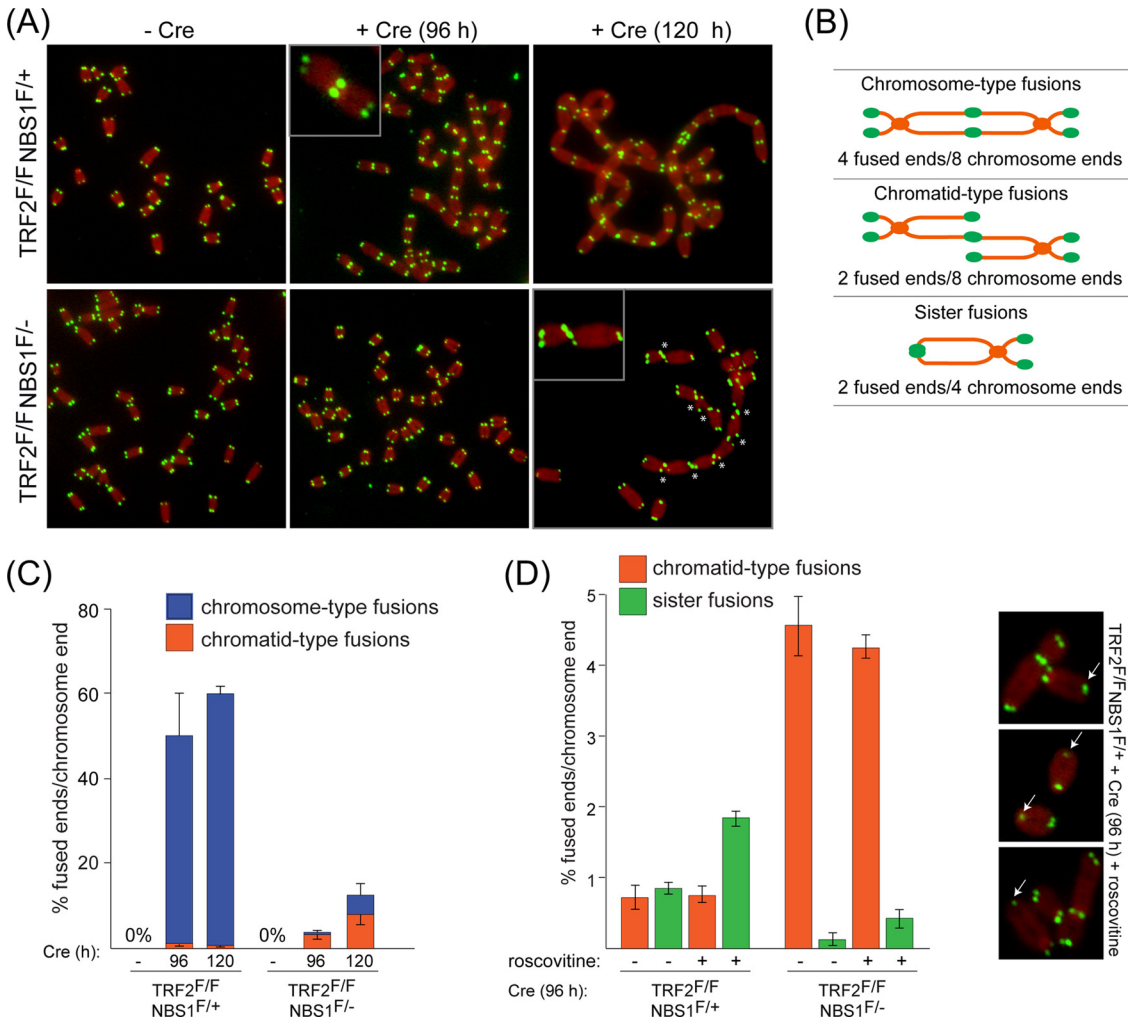

FIG. 2. Effect of NBS1 deficiency on telomere fusions. (A) Metaphase spreads from TRF2$^{F/F}$ NBS1$^{F/+}$ and TRF2$^{F/F}$ NBS1$^{F/-}$ MEFs, harvested untreated or 96 and 120 h after Cre infection. Telomeric signals were detected with FITC-OO-(CCCTAA)$_3$ oligonucleotide (green), and DNA was stained with DAPI (red). Enlarged panels show representative chromosome- and chromatid-type fusions. (B) Schematic of the method used to determine the frequency of fused ends in metaphase spreads containing chromosome-type, chromatid-type, and sister telomere fusion events. (C) Quantification of the frequency of chromosome ends engaged in chromosome- and chromatid-type fusions, scored as described for panel B, in metaphase spreads of cells shown in panel A. Bars represent averages of results from three independent experiments, and error bars indicate standard deviations. At least 2,000 chromosome ends were scored for each cell line and treatment. (D) Quantification of the frequency of chromosome ends engaged in chromatid-type and sister telomere fusions, scored as described for panel B, in metaphase spreads of TRF2$^{F/F}$ NBS1$^{F/+}$ and TRF2$^{F/F}$ NBS1$^{F/-}$ MEFs, harvested at 96 h after Cre treatment, in the presence or absence of 50 μM roscovitine for 4 h prior to harvesting. Error bars represent standard deviations from the average values for three independent experiments. At least 2,000 chromosome ends were scored for each cell line and treatment.

that more than 90% of the NHEJ events detected in metaphase spreads of control NBS1-proficient cells lacking TRF2 were chromosome-type fusions (Fig. 2A to C). In contrast, only 20 to 30% of the fusion events detected in metaphase spreads of TRF2/NBS1-deficient cells were of the chromosome type (Fig. 2A to C). When chromatid- and chromosome-type fusions were scored separately, we found that deficiency in NBS1 was associated with a >10-fold suppression in the occurrence of chromosome-type fusions, arguing that NBS1 is required for the majority of telomere NHEJ events in G_1. This result is consistent with the requirement for NBS1 in ATM signaling, since repression of G_1 telomere fusions was also observed in TRF2/ATM-deficient cells (see below). This diminished efficiency of NHEJ at dysfunctional telomeres in G_1 is likely due to the lack of 53BP1-mediated telomere mobility (18).

Absence of H2AX also affected the frequency of telomere fusions, but to a lesser extent. We observed a five- to sevenfold reduction in the frequency of NHEJ when TRF2 was removed in H2AX-deficient cells (see Fig. S2 and S3A and B in the supplemental material), consistent with the phenotype observed in cells deficient for MDC1 and in cells where MDC1 or H2AX protein levels were downregulated by RNA interference (18, 19). Most likely, the abilities of γ-H2AX to amplify the ATM signal and to promote the MDC1-mediated accumulation of 53BP1 in TIFs are relevant to its contribution to the NHEJ pathway.

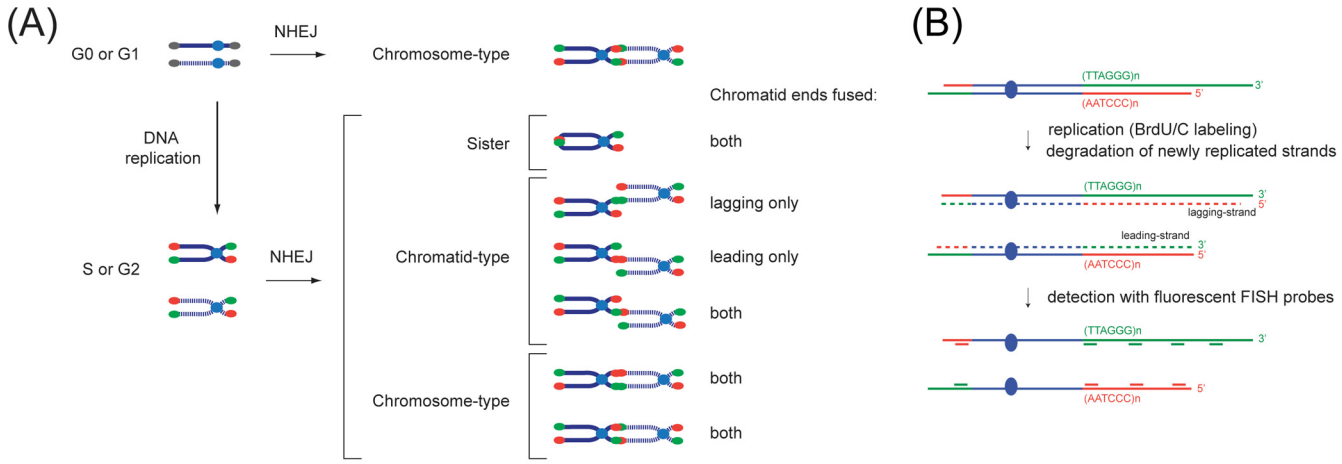

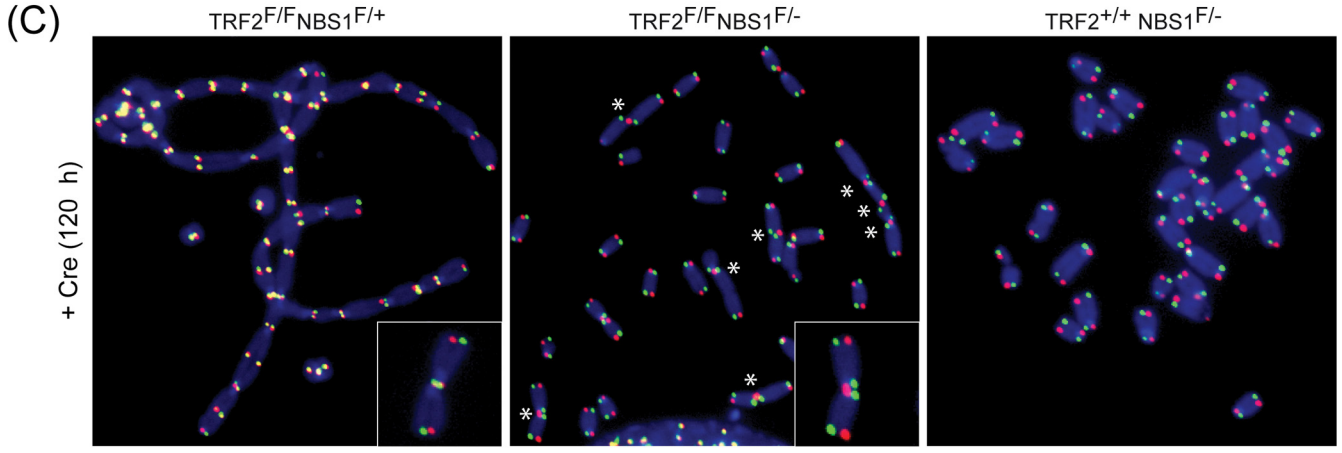

(D)

+ Cre (120 h)	Chromosome ends scored	Chromatid ends fused (% of chr. ends)	Leading ends only (% of chr. ends)
$TRF2^{F/F}NBS1^{F/+}$	3868	2 (0.1%)	2 (0.1%)
$TRF2^{F/F}NBS1^{F/-}$	4678	350 (7.5%)	350 (7.5%)
$TRF2^{+/+}NBS1^{F/-}$	3112	10 (0.3%)	6 (0.2%)

FIG. 3. NBS1 prevents the fusions of telomeres generated by leading-strand DNA synthesis. (A) Schematic of the possible telomere fusion events that can be detected in metaphase spreads. (Top) The fusion of dysfunctional telomeres before replication (G_0 or G_1) leads to the occurrence of chromosome-type fusions in metaphase spreads. (Bottom) Postreplicative (S or G_2) repair of dysfunctional telomeres can give rise to sister, chromosome-type, or chromatid-type telomere fusions. The different combinations of joining events between leading- and lagging-strand chromatids are indicated. (B) Schematic of the CO-FISH method used to differentiate telomeres resulting from leading- and lagging-strand DNA synthesis. (C) Metaphase spreads of $TRF2^{F/F}$ $NBS1^{F/+}$, $TRF2^{F/F}$ $NBS1^{F/-}$, and $TRF2^{+/+}$ $NBS1^{F/-}$ MEFs, analyzed by CO-FISH at 120 h after Cre treatment. Telomeric signals on the leading strand were detected with TAMRA-OO-$(TTAGGG)_3$ oligonucleotide (red) and costained with FITC-OO-$(CCCTAA)_3$ probe (green) specific to lagging-strand telomeres; DNA was stained with DAPI (blue). Enlarged panels show representative fusion events. (D) Table showing the chromatid-type fusions detected in metaphase spreads of Cre-treated $TRF2^{F/F}$ $NBS1^{F/+}$, $TRF2^{F/F}$ $NBS1^{F/-}$, and $TRF2^{+/+}$ $NBS1^{F/-}$ cells (shown in panel C). The total number of chromosome ends, the number of chromatid ends fused, and the number of leading ends fused to leading ends are indicated. The data were confirmed in an independent experiment. At least 3,000 chromosome ends were scored for each cell line.

MRN and TRF2 repress NHEJ of telomeres formed by leading-strand synthesis. The prevalent type of fusions in Cre-treated $TRF2^{F/F}$ $NBS1^{F/-}$ cells was the chromatid type, indicative of postreplicative repair in S/G_2 (Fig. 2A to C). Postreplicative fusions were rarely observed in H2AX-deficient cells (see Fig. S3A and B in the supplemental material), suggesting that MRN, but not H2AX, acts to prevent the NHEJ pathway from engaging dysfunctional telomeres in late S/G_2.

One of the possible postreplicative fusion events is the joining of the telomeres of sister chromatids (sister telomere fusions) (see schematic in Fig. 3A). Sister telomere fusions require that the NHEJ reaction joins a telomere formed by leading-strand DNA synthesis and one formed by lagging-

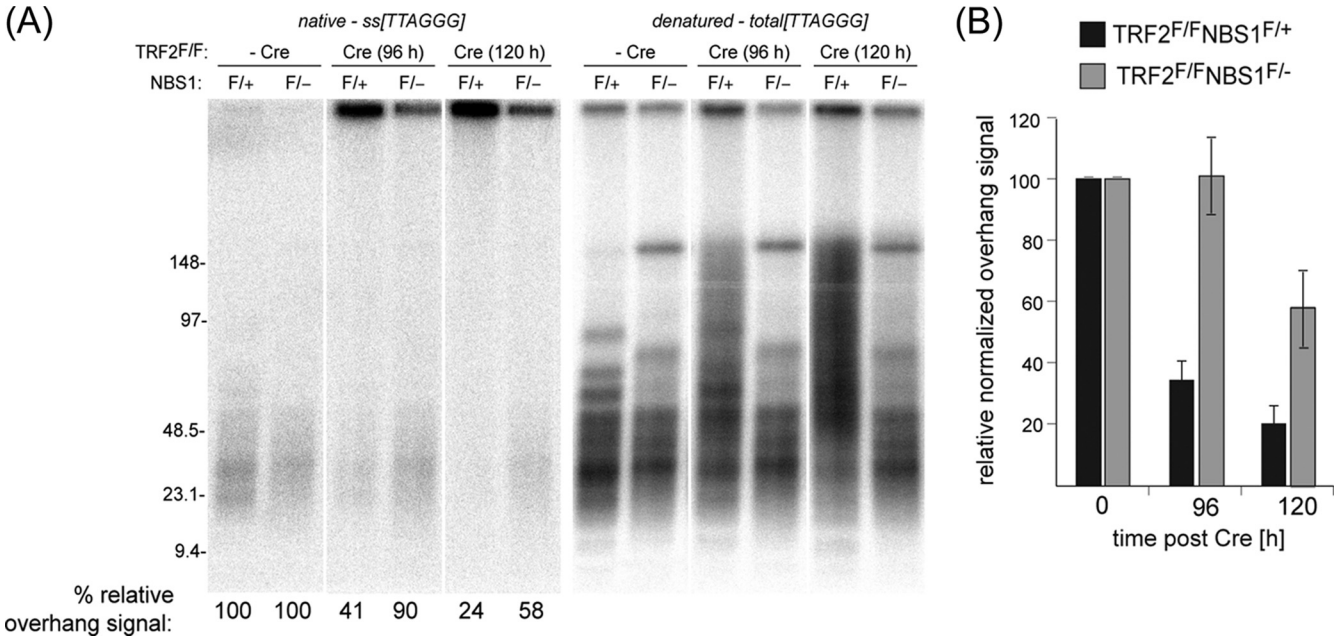

FIG. 4. Telomeric overhangs in TRF2- and NBS1-deficient cells. (A) Telomeric DNA analysis. (Left) In-gel assay detecting 3′ overhang of $TRF2^{F/F}$ $NBS1^{F/+}$ and $TRF2^{F/F}$ $NBS1^{F/-}$ MEFs, harvested untreated or 96 and 120 h after infection with Cre and processed by in-gel hybridization to a $(CCCTAA)_4$ probe to detect single-stranded TTAGGG repeats (native). (Right) The DNA was denatured in situ and rehybridized to the same probe to detect the total TTAGGG signal (denatured). Overhang signals were quantified with ImageQuant software and normalized to the total TTAGGG signal in the same lane. The numbers below the gel represent the percentages of normalized overhang signal compared to the normalized overhang signal for the same cells not treated with Cre. (B) Quantification of telomeric overhang at 0, 96, and 120 h after infection with Cre in five independent experiments. The overhang signals at different time points after Cre infection are represented as percentages of the overhang signal in the absence of Cre for the same cell line.

strand DNA synthesis. As sister fusions were rarely observed in the TRF2/NBS1 double-knockout setting (Fig. 2D), we considered that either the lagging-strand end or the leading-strand end remained protected from NHEJ.

We further characterized the chromatid-type fusions observed upon loss of TRF2 and NBS1 by using CO-FISH (3), which can differentiate between the telomeres generated by leading- and lagging-strand DNA synthesis (Fig. 3A and B). Without exception, the chromatid fusions observed in $TRF2^{F/F}$ $NBS1^{F/-}$ cells at 120 h after Cre treatment involved the joining of two leading-strand telomeres (Fig. 3C and D). Since G_2 telomere fusions rarely occur as a consequence of TRF2 deletion alone (Fig. 2; see also Fig. S4 in the supplemental material) or deletion of NBS1 alone (Fig. 3C and D), there appear to be at least two independent pathways that protect leading-strand telomeres from fusion in G_2: one requiring TRF2 (but not NBS1 or not NBS1 alone) and one involving NBS1 (independent of TRF2).

Telomeres formed by leading-strand DNA synthesis are likely to be initially blunt, whereas telomeres formed by lagging-strand DNA synthesis are predicted to have a short 3′ extension after the removal of the last primer for lagging-strand synthesis. To generate the telomeric overhang, which is required for telomere function, telomere ends are thought to be processed after each round of DNA replication. Based on these considerations, we asked whether Nbs1 might be required for overhang generation at leading-strand telomeres after replication in cells that lack TRF2. We therefore analyzed the telomeric overhang in $NBS1^{F/-}$, $TRF2^{F/F}$ $NBS1^{F/+}$, and $TRF2^{F/F}$ $NBS1^{F/-}$ cells at 96 and 120 h after Cre infection by in-gel hybridization (Fig. 4A and data not shown). Nbs1 loss by itself did not lead to a significant change in overhang signal (data not shown). As expected, TRF2 deletion in NBS1-proficient cells resulted in a progressive decrease in overhang signal that roughly correlated with the frequency of telomere fusions at each time point (Fig. 4A and B). At 96 h after Cre treatment, only 35% ± 7% of the overhang signal was detectable (Fig. 4B) and the corresponding amount of overhang loss (65% ± 7%) was comparable to the frequency of chromosome end fusions observed at the same time point (50% ± 10%) (Fig. 3D). Similarly, at 120 h after Cre treatment, as more telomere fusions were formed (60% ± 2%) (Fig. 3D), the overhang signal decreased to 21% ± 6% (equivalent to a 79% ± 6% overhang loss) (Fig. 4B). These data are consistent with the coupling between overhang loss and telomere fusions that occur in TRF2-depleted mouse cells (19).

In the TRF2/NBS1-deficient setting, there was much less overall overhang loss, as expected on the basis of the lower level of telomere fusions. However, it appeared that in the absence of Nbs1 and TRF2, there was a greater level of overhang loss (41% ± 12% at 120 h after Cre treatment) (Fig. 4B) than would be expected on the basis of the occurrence of telomere fusions (13% ± 3% at 120 h after Cre treatment) (Fig. 2C). This result would be consistent with a deficiency in the generation of the overhang at leading-strand telomeres when cells lack TRF2 and NBS1. However, the findings would need to be further confirmed in a setting where no telomere

fusions occur (e.g., TRF2/NBS1/DNA ligase IV triple knockout), thus avoiding confounding aspects of overhang loss during NHEJ.

A previous study had implicated cyclin-dependent kinase activity in the repression of postreplicative DNA ligase IV-dependent NHEJ of dysfunctional telomeres generated by deletion of TRF2 (25) (Fig. 2D). Importantly, roscovitine induces sister telomere fusions, indicating that Cdk1 inhibition renders both the lagging- and leading-strand telomeres sensitive to NHEJ. We therefore asked whether roscovitine affected the leading-strand fusions found in NBS1/TRF2-deficient cells. The frequency of chromatid-type fusions in NBS1/TRF2-deficient cells was not increased by roscovitine (Fig. 2D), suggesting that NBS1 is in the same pathway as Cdk1 with regard to protection of the leading-strand ends and that the MRN complex might be the relevant Cdk1 target in this setting. It is puzzling, however, that roscovitine did not induce sister telomere fusions in NBS1/TRF2-deficient cells whereas it had the expected effect in TRF2-null cells and in TRF2/H2AX-deficient cells (Fig. 2D; see also Fig. S3C in the supplemental material). Thus, when NBS1 is absent, the lagging-strand telomeres fail to fuse to their leading-strand sisters, even though their protection is breached by treatment with roscovitine. One interpretation of this result is that NBS1 contributes to a step required specifically for the NHEJ reaction involving lagging-strand telomeres that is not required when leading-strand ends are fused.

ATM and NBS1 have the same effect on telomere NHEJ in G_2. We next asked whether in the context of TRF2 deletion ATM-null cells gave rise to a phenotype similar to that observed in NBS1-deficient cells (Fig. 5A). In metaphase spreads of $TRF2^{F/-}$ $ATM^{-/-}$ MEFs analyzed at 120 h after Cre treatment, we observed that approximately 9% of the chromosome ends were engaged in leading- to leading-end chromatid-type fusions, compared to less than 1% in control cells (Fig. 5B to D), indicating that deficiencies in ATM and NBS1 give rise to the same phenotype. In both settings, we also observed low frequencies of chromosome-type fusions at the later time points. We consider it likely that these fusions represent chromosomes with a prior G_2 chromatid-type fusion event that underwent nondisjunction followed by replication of the fusion point in the next cell cycle.

In order to address whether the G_2 fusion events were in fact due to NHEJ, we generated $TRF2^{F/-}$ $ATM^{-/-}$ $Lig4^{-/-}$ cells which lack the major ligase responsible for NHEJ, DNA ligase IV (Fig. 5B). In the absence of DNA ligase IV, the incidence of chromatid-type fusions was reduced at least ninefold at the late, 120-h time point after Cre treatment (Fig. 5C and D), indicating that the majority of fusions was a consequence of NHEJ. On the basis of these findings, we conclude that leading-strand telomeres are vulnerable to processing by the NHEJ pathway after replication. Furthermore, the data suggest that the MRN/ATM pathway and TRF2 can independently provide telomere protection during the G_2 stage of the cell cycle.

DISCUSSION

MRN as the sensor in the ATM pathway. Our results strongly argue in favor of the view that the MRN complex is required for the activation of ATM at dysfunctional telomeres. The data establish that no other activity, at least no other activity present in the MEFs studied here, can activate the ATM kinase signaling cascade at telomeres lacking TRF2. The conclusion that MRN is the only sensor for the ATM pathway is consistent with a body of work published previously (reviewed in references 34 and 35) and with recent data that showed a strong (but incomplete) dependence of DNA damage signaling on Mre11 in the context of telomere dysfunction generated by a dominant-negative allele of the shelterin component TPP1 (6). The strength of the system used here is that it affords a more precise parsing of the role of MRN in the ATM pathway, as deletion of TRF2 does not activate other signaling pathways.

Mounting evidence indicates that the molecular events that take place at deprotected telomeres recapitulate the sequence of events that occur in response to chromosome-internal DSBs, including the activation of checkpoint signaling, the recruitment of DNA damage response factors, and the NHEJ-mediated repair of the DNA ends (reviewed in reference 32). On the basis of the extent of this parallel, we consider it likely that the requirement for MRN in ATM activation is not a unique feature of dysfunctional telomeres but pertains to all DSBs.

How telomeres block the ATM pathway and NHEJ. The demonstration that MRN is required for ATM signaling at dysfunctional telomeres now suggests a model for the mechanism by which telomeres solve this aspect of the end protection problem. As TRF2 is required for prevention of activation of ATM at telomeres, it might act by repressing the MRN sensor step. MRN is known to engage DNA ends, and this feature is generally assumed to be the critical mechanism by which MRN detects DSBs (27). One obvious way by which telomeres might avoid alerting MRN/ATM is by sequestering the chromosome end in the t-loop configuration. TRF2 has been implicated in the formation of the t-loop structure (21, 42), although this role has not been demonstrated in vivo. If TRF2 is indeed required for the formation and/or maintenance of t-loops, a model whereby TRF2 generates t-loops, which prevent the activation of the ATM pathway by simply blocking MRN from engaging the chromosome end, can be proposed (Fig. 6A).

This model is analogous to that proposed for the inhibition of NHEJ, which posited that t-loops prevent the Ku heterodimer from gaining access to the chromosome end (11, 15). Since both the Ku heterodimer and the MRN/ATM pathway contribute to NHEJ of dysfunctional telomeres, we can now expand this model and suggest that t-loops, by blocking two types of DNA end binding activities, MRN and Ku70/80, block the initiation and execution of this detrimental repair pathway at natural chromosome ends (Fig. 6A).

Contribution of MRN/ATM to NHEJ. The contribution of the MRN/ATM pathway to the execution of NHEJ in G_1 can be explained through its ability to promote 53BP1-mediated chromatin mobility, which facilitates the fusion of uncapped chromosome ends (18). However, deficiency in ATM or MRN results in a more severe NHEJ phenotype than the absence of H2AX or MDC1, both of which act downstream of ATM/MRN to promote accumulation of 53BP1 at dysfunctional telomeres. One explanation is that the massive 53BP1 accumulation required for cytological detection is in excess of the requirement for NHEJ. Perhaps the phosphorylation of a lim-

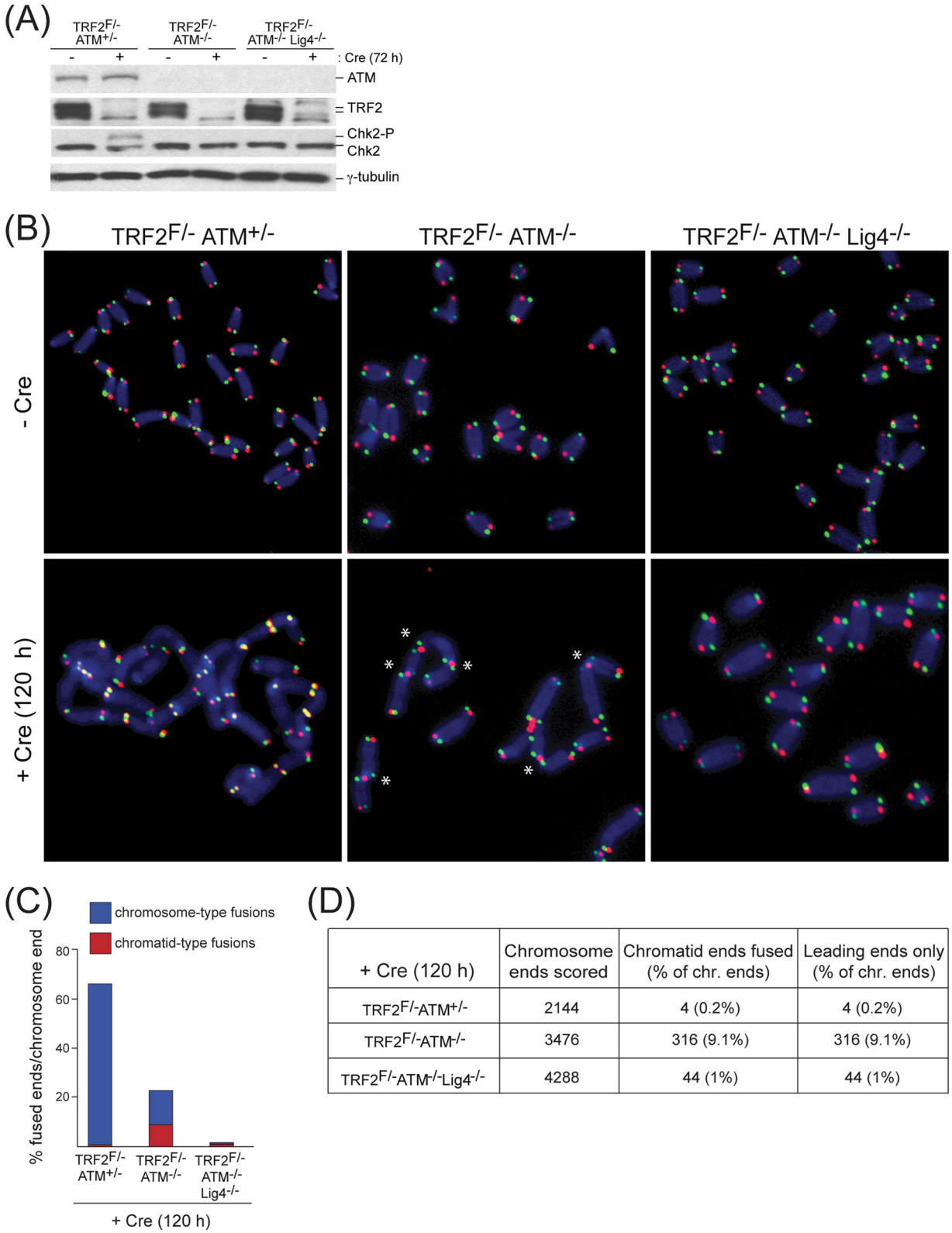

+ Cre (120 h)	Chromosome ends scored	Chromatid ends fused (% of chr. ends)	Leading ends only (% of chr. ends)
$TRF2^{F/-}ATM^{+/-}$	2144	4 (0.2%)	4 (0.2%)
$TRF2^{F/-}ATM^{-/-}$	3476	316 (9.1%)	316 (9.1%)
$TRF2^{F/-}ATM^{-/-}Lig4^{-/-}$	4288	44 (1%)	44 (1%)

FIG. 5. ATM protects leading-strand telomeres from processing by NHEJ upon loss of TRF2. (A) Immunoblot detection of ATM, TRF2, and Chk2 in $TRF2^{F/-}$ $ATM^{+/-}$, $TRF2^{F/-}$ $ATM^{-/-}$, and $TRF2^{F/-}$ $ATM^{-/-}$ $Lig4^{-/-}$ MEFs untreated or 72 h after Cre infection. γ-Tubulin was used as a loading control. ∗ indicates a nonspecific band. (B) Metaphase spreads of $TRF2^{F/-}$ $ATM^{+/-}$, $TRF2^{F/-}$ $ATM^{-/-}$, and $TRF2^{F/-}$ $ATM^{-/-}$ $Lig4^{-/-}$ MEFs, analyzed by CO-FISH untreated or 120 h after Cre treatment. Telomeric signals on the leading strand were detected with TAMRA-OO-$(TTAGGG)_3$ oligonucleotide (red) and costained with a lagging-strand telomere-specific FITC-OO-$(CCCTAA,)_3$ probe (green); DNA was stained with DAPI (blue). (C) Quantification of chromosome- and chromatid-type fusions detected in metaphase spreads of cells shown in panel B. (D) Table showing the chromatid-type fusions detected in metaphase spreads shown in panel B and scored in panel C. The total number of chromosome ends, the number of chromatid ends fused, and the number of leading ends fused to leading ends are indicated. At least 2,000 chromosome ends were scored for each cell line.

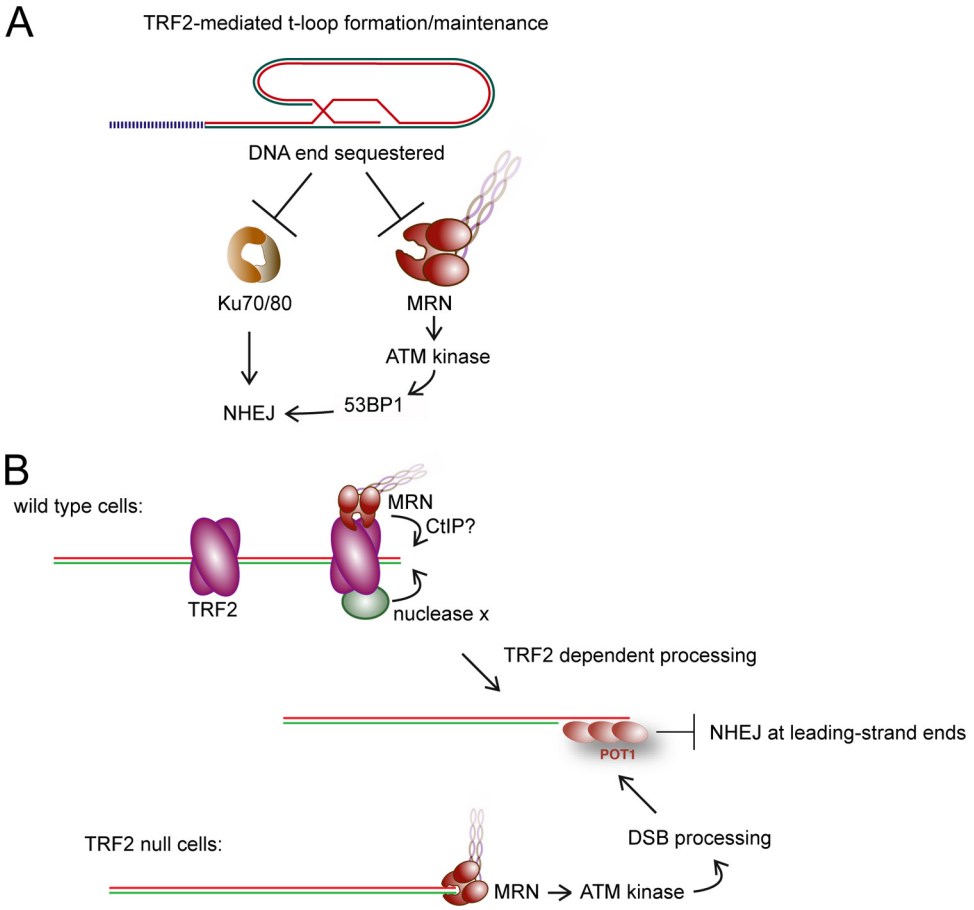

FIG. 6. Model for the dual role of MRN/ATM at functional and dysfunctional telomeres. (A) At functional telomeres, prior to replication, TRF2-mediated t-loop formation or maintenance is proposed to block the loading of Ku70/80 and MRN onto telomeric DNA, thus protecting chromosome ends from processing by NHEJ and from activating ATM signaling. (B) Model for repression of NHEJ at telomeres replicated by leading-strand DNA synthesis. After replication, TRF2 is proposed to promote overhang generation by recruiting MRN and an unknown nuclease(s), both of which have the ability to resect blunt telomeres generated by leading-strand DNA synthesis. The overhang may block NHEJ through its interaction with POT1. In the absence of TRF2, MRN/ATM-dependent DSB processing of dysfunctional telomeres also generates resected ends that can bind POT1 and are protected from NHEJ.

ited amount of 53BP1, mediated by the MRN/ATM pathway, may be sufficient to promote NHEJ but not to yield detectable 53BP1 foci. Since deficiency in H2AX or MDC1 moderates but does not abrogate the ATM signaling pathway at dysfunctional telomeres, sufficient phosphorylated 53BP1 might be present for sustenance of NHEJ, albeit at a slower pace.

Our data also show that NHEJ can take place in the absence of MRN/ATM. Specifically, the postreplicative fusions involving leading-strand ends do not require NBS1 or ATM. We consider it possible, however, that the lack of ATM signaling in this setting and the presumed lack of signaling by other phosphoinositide-3-kinase-related protein kinases diminish the frequency of the leading-end fusions. Indeed, the leading-end fusions are rare (involving a third of the leading-end telomeres), even in TRF2/NBS1- and TRF2/ATM-null cells. It would be of interest to examine the effect of a dissociation of function mutation in the MRN complex that abrogates the proposed end-processing activity but retains the ability to activate the ATM signaling pathway. Such mutants are not yet available.

Contribution of MRN/ATM to telomere protection. Our data now also shed light on the paradoxical presence of the MRN complex at telomeres. Mre11 and Rad50 are at telomeres throughout the cell cycle, with Nbs1 joining the complex at telomeres in S phase (57). Since MRN interacts with TRF2, it appeared that its presence at telomeres is actively promoted by shelterin. Given that MRN promotes two undesirable events at chromosome ends, ATM signaling and NHEJ, the question is why shelterin has evolved the ability to bring this complex to telomeres.

In this study, we present evidence that the MRN/ATM pathway can protect telomeres from NHEJ, specifically after DNA replication. This protective feature was observed only at telomeres generated by leading-strand DNA synthesis, resulting in leading-end fusions in TRF2/NBS1- or TRF2/ATM-deficient cells. The inability of MRN and ATM to protect the telomeres generated by leading-strand DNA synthesis is observed only when TRF2 is absent, indicating that in the presence of TRF2, MRN/ATM is not the only protective factor at the leading-strand ends.

To explain these observations, we propose a model for the protection of telomeres generated by leading-strand synthesis that focuses on the generation of the telomeric overhang as the main mechanism by which NHEJ is repressed in G_2 (Fig. 6B). It is likely that the presence of a telomeric overhang can help to protect telomeres from NHEJ by recruiting POT1 proteins, which may simply block the Ku heterodimer from loading on the DNA end. Indeed, in the absence of POT1a and POT1b, mouse telomeres undergo infrequent but detectable fusions after DNA replication (23). In that setting, both the lagging- and the leading-strand ends are processed by NHEJ, often resulting in sister fusions. Thus, immediately after DNA replication, perhaps before t-loops are reformed, it appears that POT1 loading on the 3′ overhang may inhibit telomere fusions (Fig. 6B).

We propose that both TRF2 and MRN contribute to the 5′ end resection necessary for the overhang formations at the ends formed by leading-strand DNA synthesis, which, unlike the telomere formed by lagging-strand DNA synthesis, is not expected to have an overhang immediately after DNA replication. TRF2 might promote resection through recruitment of MRN and its associated presumed nuclease, CtIP (39, 45). Perhaps the interaction between TRF2 and MRN is such that it allows processing but blocks activation of the ATM kinase. TRF2 is likely to have additional associated activities that can fulfill this role since NBS1-deficient cells do not show leading-end fusions as long as TRF2 is present. The second TRF2-dependent (but MRN/ATM-independent) activity responsible for resection will be of interest. It should be noted that DNA-protein kinase activity has also been implicated in the protection of leading-strand ends from fusion (4). The target of the DNA-protein kinase in this context is not yet known, but CtIP may be a candidate.

When TRF2 is absent, MRN may still be able to fulfill the same processing function, but now as a consequence of activation of ATM at the deprotected chromosome end. Thus, although ATM activation is detrimental and nonphysiological, this pathological setting reveals the protective features of end processing by MRN that are not normally seen, due to redundancy in the TRF2-mediated processing of the leading-end telomeres. This highly speculative model predicts that if the additional end-processing activities brought in by TRF2 are known, the combination of their absence with MRN deficiency will reveal a high incidence of leading-end chromatid-type telomere fusions. We are currently testing this model.

TRF2ΔBΔM allele revisited. Chromatid-type leading- to leading-strand telomere fusions have been described as a prominent outcome of telomere dysfunction, induced by the overexpression of a dominant-negative allele of TRF2, TRF2ΔBΔM in human cells (2, 41, 47). The TRF2ΔBΔM allele lacks the Myb-type DNA binding domain (M) and the N-terminal basic GAR region (B) and acts by binding to endogenous TRF2 and sequestering it away from chromosome ends. However, since TRF2ΔBΔM retains the interaction with the MRN complex, overexpression of this dominant-negative allele also prevents the association of MRN with chromosome ends (57). Therefore, the chromatid-type fusions, incurred by TRF2ΔBΔM overexpression, are likely due to the combined absence of both TRF2 and MRN from telomeres, similarly to the situation described here for codeletion of TRF2 and NBS1.

ACKNOWLEDGMENTS

We are grateful to Andre Nussenzweig for his generous gift of H2AX-deficient and NBS1-conditional knockout mice. We thank Eros Lazzerini Denchi for the TRF2/ATM/Lig4 MEFs and Devon White for expert mouse husbandry. John Petrini is thanked for Nbs1 antibodies and communication of unpublished results. Junjie Chen is thanked for MDC1 antibodies. Members of the de Lange laboratory are thanked for helpful discussion of this work.

This work was supported by a grant from the NIH (R37 GM049046). N.D. was supported by an HHMI predoctoral fellowship.

REFERENCES

1. **Bai, Y., and J. P. Murnane.** 2003. Telomere instability in a human tumor cell line expressing NBS1 with mutations at sites phosphorylated by ATM. Mol. Cancer Res. **1:**1058–1069.
2. **Bailey, S. M., M. N. Cornforth, A. Kurimasa, D. J. Chen, and E. H. Goodwin.** 2001. Strand-specific postreplicative processing of mammalian telomeres. Science **293:**2462–2465.
3. **Bailey, S. M., E. H. Goodwin, and M. N. Cornforth.** 2004. Strand-specific fluorescence in situ hybridization: the CO-FISH family. Cytogenet. Genome Res. **107:**14–17.
4. **Bailey, S. M., M. A. Brenneman, J. Halbrook, J. A. Nickoloff, R. L. Ullrich, and E. H. Goodwin.** 2004. The kinase activity of DNA-PK is required to protect mammalian telomeres. DNA Repair (Amsterdam) **3:**225–233.
5. **Bassing, C. H., K. F. Chua, J. Sekiguchi, H. Suh, S. R. Whitlow, J. C. Fleming, B. C. Monroe, D. N. Ciccone, C. Yan, K. Vlasakova, D. M. Livingston, D. O. Ferguson, R. Scully, and F. W. Alt.** 2002. Increased ionizing radiation sensitivity and genomic instability in the absence of histone H2AX. Proc. Natl. Acad. Sci. USA **99:**8173–8178.
6. **Buis, J., Y. Wu, Y. Deng, J. Leddon, G. Westfield, M. Eckersdorff, J. M. Sekiguchi, S. Chang, and D. O. Ferguson.** 2008. Mre11 nuclease activity has essential roles in DNA repair and genomic stability distinct from ATM activation. Cell **135:**85–96.
7. **Burma, S., B. P. Chen, M. Murphy, A. Kurimasa, and D. J. Chen.** 2001. ATM phosphorylates histone H2AX in response to DNA double-strand breaks. J. Biol. Chem. **276:**42462–42467.
8. **Celeste, A., O. Fernandez-Capetillo, M. J. Kruhlak, D. R. Pilch, D. W. Staudt, A. Lee, R. F. Bonner, W. M. Bonner, and A. Nussenzweig.** 2003. Histone H2AX phosphorylation is dispensable for the initial recognition of DNA breaks. Nat. Cell Biol. **5:**675–679.
9. **Celeste, A., S. Petersen, P. J. Romanienko, O. Fernandez-Capetillo, H. T. Chen, O. A. Sedelnikova, B. Reina-San-Martin, V. Coppola, E. Meffre, M. J. Difilippantonio, C. Redon, D. R. Pilch, A. Olaru, M. Eckhaus, R. D. Camerini-Otero, L. Tessarollo, F. Livak, K. Manova, W. M. Bonner, M. C. Nussenzweig, and A. Nussenzweig.** 2002. Genomic instability in mice lacking histone H2AX. Science **296:**922–927.
10. **Celli, G., and T. de Lange.** 2005. DNA processing is not required for ATM-mediated telomere damage response after TRF2 deletion. Nat. Cell Biol. **7:**712–718.
11. **Celli, G. B., E. Lazzerini Denchi, and T. de Lange.** 2006. Ku70 stimulates fusion of dysfunctional telomeres yet protects chromosome ends from homologous recombination. Nat. Cell Biol. **8:**885–890.
12. **Chai, W., A. J. Sfeir, H. Hoshiyama, J. W. Shay, and W. E. Wright.** 2006. The involvement of the Mre11/Rad50/Nbs1 complex in the generation of G-overhangs at human telomeres. EMBO Rep. **7:**225–230.
13. **de Jager, M., M. L. Dronkert, M. Modesti, C. E. Beerens, R. Kanaar, and D. C. van Gent.** 2001. DNA-binding and strand-annealing activities of human Mre11: implications for its roles in DNA double-strand break repair pathways. Nucleic Acids Res. **29:**1317–1325.
14. **de Jager, M., J. van Noort, D. C. van Gent, C. Dekker, R. Kanaar, and C. Wyman.** 2001. Human Rad50/Mre11 is a flexible complex that can tether DNA ends. Mol. Cell **8:**1129–1135.
15. **de Lange, T.** 2005. Shelterin: the protein complex that shapes and safeguards human telomeres. Genes Dev. **19:**2100–2110.
16. **de Lange, T., and J. Petrini.** 2000. A new connection at human telomeres: association of the Mre11 complex with TRF2. Cold Spring Harbor Symp. Quant. Biol. **LXV:**265–273.
17. **Difilippantonio, S., A. Celeste, O. Fernandez-Capetillo, H. T. Chen, B. Reina San Martin, F. Van Laethem, Y. P. Yang, G. V. Petukhova, M. Eckhaus, L. Feigenbaum, K. Manova, M. Kruhlak, R. D. Camerini-Otero, S. Sharan, M. Nussenzweig, and A. Nussenzweig.** 2005. Role of Nbs1 in the activation of the Atm kinase revealed in humanized mouse models. Nat. Cell Biol. **7:**675–685.
18. **Dimitrova, N., Y. C. Chen, D. L. Spector, and T. de Lange.** 2008. 53BP1 promotes non-homologous end joining of telomeres by increasing chromatin mobility. Nature **456:**524–528.

19. **Dimitrova, N., and T. de Lange.** 2006. MDC1 accelerates nonhomologous end-joining of dysfunctional telomeres. Genes Dev. **20:**3238–3243.
20. **Franco, S., M. Gostissa, S. Zha, D. B. Lombard, M. M. Murphy, A. A. Zarrin, C. Yan, S. Tepsuporn, J. C. Morales, M. M. Adams, Z. Lou, C. H. Bassing, J. P. Manis, J. Chen, P. B. Carpenter, and F. W. Alt.** 2006. H2AX prevents DNA breaks from progressing to chromosome breaks and translocations. Mol. Cell **21:**201–214.
21. **Griffith, J. D., L. Comeau, S. Rosenfield, R. M. Stansel, A. Bianchi, H. Moss, and T. de Lange.** 1999. Mammalian telomeres end in a large duplex loop. Cell **97:**503–514.
22. **Helmink, B. A., A. L. Bredemeyer, B. S. Lee, C. Y. Huang, G. G. Sharma, L. M. Walker, J. J. Bednarski, W. L. Lee, T. K. Pandita, C. H. Bassing, and B. P. Sleckman.** 2009. MRN complex function in the repair of chromosomal Rag-mediated DNA double-strand breaks. J. Exp. Med. **206:**669–679.
23. **Hockemeyer, D., J. P. Daniels, H. Takai, and T. de Lange.** 2006. Recent expansion of the telomeric complex in rodents: two distinct POT1 proteins protect mouse telomeres. Cell **126:**63–77.
24. **Hopfner, K. P., L. Craig, G. Moncalian, R. A. Zinkel, T. Usui, B. A. Owen, A. Karcher, B. Henderson, J. L. Bodmer, C. T. McMurray, J. P. Carney, J. H. Petrini, and J. A. Tainer.** 2002. The Rad50 zinc-hook is a structure joining Mre11 complexes in DNA recombination and repair. Nature **418:**562–566.
25. **Konishi, A., and T. de Lange.** 2008. Cell cycle control of telomere protection and NHEJ revealed by a ts mutation in the DNA-binding domain of TRF2. Genes Dev. **22:**1221–1230.
26. **Lazzerini Denchi, E., and T. de Lange.** 2007. Protection of telomeres through independent control of ATM and ATR by TRF2 and POT1. Nature **448:** 1068–1071.
27. **Lee, J. H., and T. T. Paull.** 2005. ATM activation by DNA double-strand breaks through the Mre11-Rad50-Nbs1 complex. Science **308:**551–554.
28. **Manolis, K. G., E. R. Nimmo, E. Hartsuiker, A. M. Carr, P. A. Jeggo, and R. C. Allshire.** 2001. Novel functional requirements for non-homologous DNA end joining in Schizosaccharomyces pombe. EMBO J. **20:**210–221.
29. **Mirzoeva, O. K., and J. H. Petrini.** 2001. DNA damage-dependent nuclear dynamics of the Mre11 complex. Mol. Cell. Biol. **21:**281–288.
30. **Moore, J. K., and J. E. Haber.** 1996. Cell cycle and genetic requirements of two pathways of nonhomologous end-joining repair of double-strand breaks in Saccharomyces cerevisiae. Mol. Cell. Biol. **16:**2164–2173.
31. **Morales, M., J. W. Theunissen, C. F. Kim, R. Kitagawa, M. B. Kastan, and J. H. Petrini.** 2005. The Rad50S allele promotes ATM-dependent DNA damage responses and suppresses ATM deficiency: implications for the Mre11 complex as a DNA damage sensor. Genes Dev. **19:**3043–3054.
32. **Palm, W., and T. de Lange.** 2008. How shelterin protects mammalian telomeres. Annu. Rev. Genet. **42:**301–334.
33. **Panier, S., and D. Durocher.** 2009. Regulatory ubiquitylation in response to DNA double-strand breaks. DNA Repair (Amsterdam) **8:**436–443.
34. **Paull, T. T., and J. H. Lee.** 2005. The Mre11/Rad50/Nbs1 complex and its role as a DNA double-strand break sensor for ATM. Cell Cycle **4:**737–740.
35. **Petrini, J., and T. H. Stracker.** 2003. The cellular response to DNA double strand breaks: defining the sensors and mediators. Trends Cell Biol. **13:**458–462.
36. **Ranganathan, V., W. F. Heine, D. N. Ciccone, K. L. Rudolph, X. Wu, S. Chang, H. Hai, I. M. Ahearn, D. M. Livingston, I. Resnick, F. Rosen, E. Seemanova, P. Jarolim, R. A. DePinho, and D. T. Weaver.** 2001. Rescue of a telomere length defect of Nijmegen breakage syndrome cells requires NBS and telomerase catalytic subunit. Curr. Biol. **11:**962–966.
37. **Reina-San-Martin, B., M. C. Nussenzweig, A. Nussenzweig, and S. Difilippantonio.** 2005. Genomic instability, endoreduplication, and diminished Ig class-switch recombination in B cells lacking Nbs1. Proc. Natl. Acad. Sci. USA **102:**1590–1595.
38. **Rodrigue, A., M. Lafrance, M. C. Gauthier, D. McDonald, M. Hendzel, S. C. West, M. Jasin, and J. Y. Masson.** 2006. Interplay between human DNA repair proteins at a unique double-strand break in vivo. EMBO J. **25:**222–231.
39. **Sartori, A. A., C. Lukas, J. Coates, M. Mistrik, S. Fu, J. Bartek, R. Baer, J. Lukas, and S. P. Jackson.** 2007. Human CtIP promotes DNA end resection. Nature **450:**509–514.
40. **Silver, D. P., and D. M. Livingston.** 2001. Self-excising retroviral vectors encoding the Cre recombinase overcome Cre-mediated cellular toxicity. Mol. Cell **8:**233–243.
41. **Smogorzewska, A., J. Karlseder, H. Holtgreve-Grez, A. Jauch, and T. de Lange.** 2002. DNA Ligase IV-dependent NHEJ of deprotected mammalian telomeres in G1 and G2. Curr. Biol. **12:**1635.
42. **Stansel, R. M., T. de Lange, and J. D. Griffith.** 2001. T-loop assembly in vitro involves binding of TRF2 near the 3′ telomeric overhang. EMBO J. **20:**5532–5540.
43. **Stucki, M., and S. P. Jackson.** 2006. gammaH2AX and MDC1: Anchoring the DNA-damage-response machinery to broken chromosomes. DNA Repair (Amsterdam) **10:**534–543.
44. **Takai, H., A. Smogorzewska, and T. de Lange.** 2003. DNA damage foci at dysfunctional telomeres. Curr. Biol. **13:**1549–1556.
45. **Takeda, S., K. Nakamura, Y. Taniguchi, and T. T. Paull.** 2007. Ctp1/CtIP and the MRN complex collaborate in the initial steps of homologous recombination. Mol. Cell **28:**351–352.
46. **van Steensel, B., and T. de Lange.** 1997. Control of telomere length by the human telomeric protein TRF1. Nature **385:**740–743.
47. **van Steensel, B., A. Smogorzewska, and T. de Lange.** 1998. TRF2 protects human telomeres from end-to-end fusions. Cell **92:**401–413.
48. **Verdun, R. E., L. Crabbe, C. Haggblom, and J. Karlseder.** 2005. Functional human telomeres are recognized as DNA damage in G2 of the cell cycle. Mol. Cell **20:**551–561.
49. **Williams, R. S., G. Moncalian, J. S. Williams, Y. Yamada, O. Limbo, D. S. Shin, L. M. Groocock, D. Cahill, C. Hitomi, G. Guenther, D. Moiani, J. P. Carney, P. Russell, and J. A. Tainer.** 2008. Mre11 dimers coordinate DNA end bridging and nuclease processing in double-strand-break repair. Cell **135:**97–109.
50. **Williams, R. S., and J. A. Tainer.** 2005. A nanomachine for making ends meet: MRN is a flexing scaffold for the repair of DNA double-strand breaks. Mol. Cell **19:**724–726.
51. **Wu, G., W. H. Lee, and P. L. Chen.** 2000. NBS1 and TRF1 colocalize at PML bodies during late S/G2 phases in immortalized telomerase-negative cells: Implication of NBS1 in alternative lengthening of telomeres. J. Biol. Chem. **275:**30618–30622.
52. **Wu, Y., S. Xiao, and X. D. Zhu.** 2007. MRE11-RAD50-NBS1 and ATM function as co-mediators of TRF1 in telomere length control. Nat. Struct. Mol. Biol. **14:**832–840.
53. **Xie, A., N. Puget, I. Shim, S. Odate, I. Jarzyna, C. H. Bassing, F. W. Alt, and R. Scully.** 2004. Control of sister chromatid recombination by histone H2AX. Mol. Cell **16:**1017–1025.
54. **Yang, Y. G., A. Saidi, P. O. Frappart, W. Min, C. Barrucand, V. Dumon-Jones, J. Michelon, Z. Herceg, and Z. Q. Wang.** 2006. Conditional deletion of Nbs1 in murine cells reveals its role in branching repair pathways of DNA double-strand breaks. EMBO J. **25:**5527–5538.
55. **Zhong, Z. H., W. Q. Jiang, A. J. Cesare, A. A. Neumann, R. Wadhwa, and R. R. Reddel.** 2007. Disruption of telomere maintenance by depletion of the MRE11/RAD50/NBS1 complex in cells that use alternative lengthening of telomeres. J. Biol. Chem. **282:**29314–29322.
56. **Zhu, J., S. Petersen, L. Tessarollo, and A. Nussenzweig.** 2001. Targeted disruption of the Nijmegen breakage syndrome gene NBS1 leads to early embryonic lethality in mice. Curr. Biol. **11:**105–109.
57. **Zhu, X. D., B. Kuster, M. Mann, J. H. Petrini, and T. de Lange.** 2000. Cell-cycle-regulated association of RAD50/MRE11/NBS1 with TRF2 and human telomeres. Nat. Genet. **25:**347–352.

LEGENDS TO SUPPLEMENTARY FIGURES

SUPPLEMENTARY FIGURE 1. H2AX is required for TIF formation and amplifies the ATM signaling pathway

(A) Effects of H2AX deletion on NBS1, MDC1, and 53BP1 TIF formation in $TRF2^{F/F}H2AX^{+/-}$ and $TRF2^{F/F}H2AX^{-/-}$ MEFs, harvested 72 h after Cre treatment and processed for IF-FISH (NBS1, MDC1, or 53BP1 [green] co-stained with telomeric TTAGGG-specific FISH probe [red]; DAPI [blue]). Images were merged and enlarged.

(B) Bar graph of the frequency of TIF positive cells. At least 150 cells processed as described in (A) were scored for 10 or more telomeric 53BP1 foci.

(C) Immunoblots detecting H2AX, TRF2, and Chk2 phosphorylation in indicated MEFs, harvested untreated or 72 h after Cre infection. γ-tubulin was used as a loading control.

SUPPLEMENTARY FIGURE 2. Lack of effect of deficiencies in H2AX or NBS1 on the proliferation of TRF2-deficient MEFs.

(A) Growth curves of $TRF2^{F/F}H2AX^{+/-}$ and $TRF2^{F/F}H2AX^{-/-}$ MEFs, plated at 24 h after mock or Cre infection and counted at the indicated time-points in two independent experiments.

(B) Growth curves of $TRF2^{F/F}NBS1^{F/+}$ and $TRF2^{F/F}NBS1^{F/-}$ MEFs derived as in (A).

SUPPLEMENTARY FIGURE 3. H2AX promotes NHEJ of dysfunctional telomeres

(A) Metaphase spreads from $TRF2^{F/F}H2AX^{+/-}$ and $TRF2^{F/F}H2AX^{-/-}$ MEFs, harvested untreated or 96 and 120 h after Cre infection. Telomeric signals were detected with FITC-OO-$(CCCTAA)_3$ oligonucleotide [green] and DNA was stained with DAPI [red]. Enlarged panel shows a representative chromosome-type fusion.

(B) Quantification of the frequency of chromosome ends engaged in chromosome- and chromatid-type fusions, scored as described in Figure 2B, in metaphase spreads of cells described in (A). Bars represent the average of three independent experiments and error bars indicated s.d. At least 2000 chromosome ends were scored for each cell line and treatment.

(C) Roscovitine induces sister telomere fusions in H2AX/TRF2-deficient cells. Quantification of the frequency of chromosome ends engaged in chromatid-type and sister telomere fusions, scored as described in Figure 2B, in metaphase spreads of $TRF2^{F/F}H2AX^{+/-}$ and $TRF2^{F/F}H2AX^{-/-}$ MEFs, harvested at 96 h after Cre treatment, in the presence or absence of 50 μM roscovitine for 4 h prior to harvesting. At least 3000 chromosome ends were scored for each cell line and treatment.

SUPPLEMENTARY FIGURE 4. Low frequency of post-replicative telomere NHEJ in TRF2-deficient, NBS1-proficient cells

Pre- and post-replicative chromosome-type fusions as well as post-replicative chromatid type fusions were analyzed by CO-FISH and the incidence of each fusion type was scored as percentage of fused ends per chromosome end. Of note, Type 2 cannot be distinguished from Type 1 but has an equal probability of occurring as Type 3 fusions and therefore is expected to occur with the same frequency as Type 3. Also, scoring Type 1 and 2 fusions may overestimate the number of G1 events as Type 4 fusions that undergo non-disjunction will appear as Type 1 and 2 events in the following metaphase.

Supplemental Figure 1 Dimitrova and de Lange

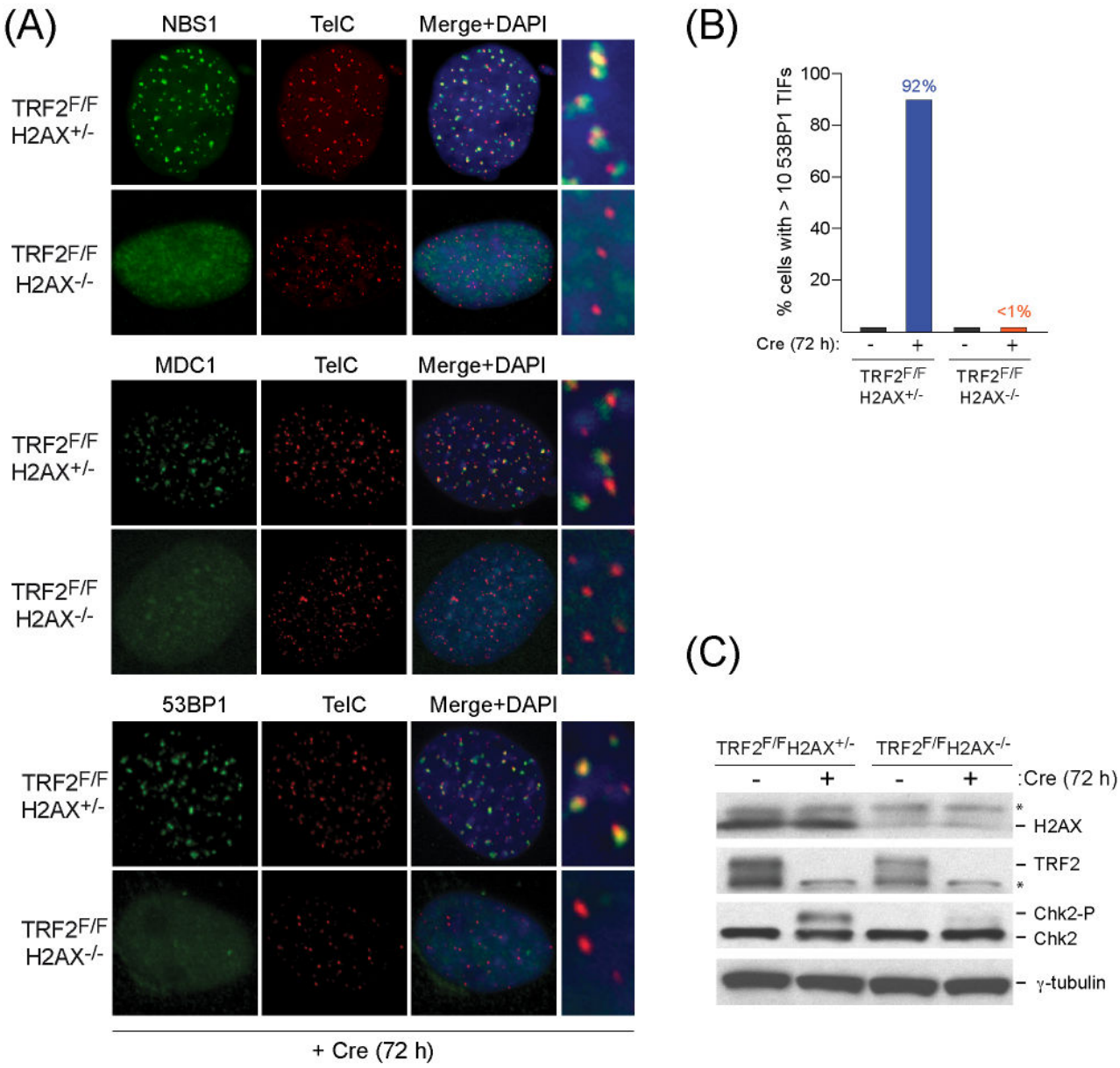

Supplementary Figure 2 Dimitrova and de Lange

(A)

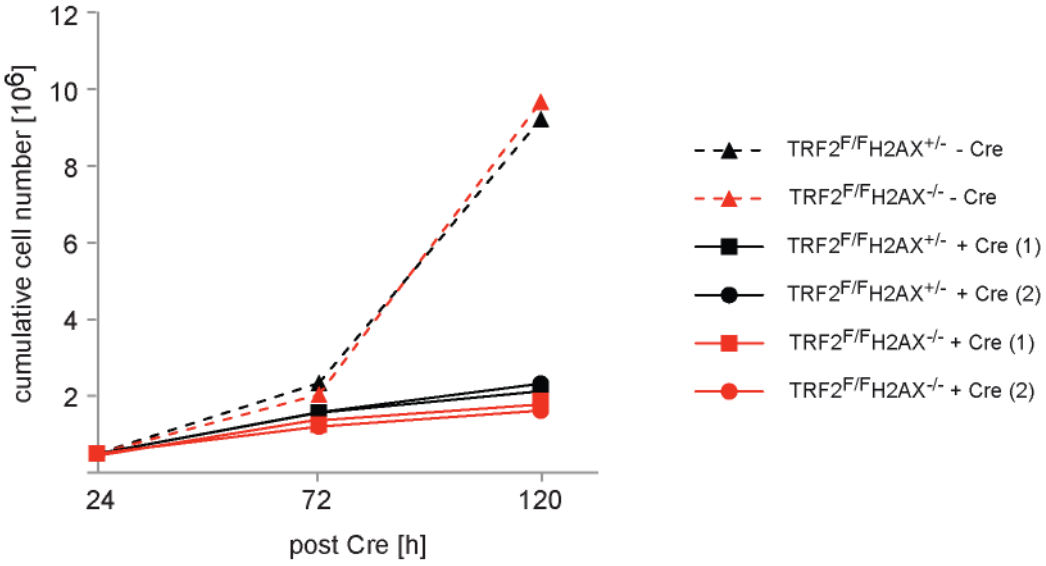

(B)

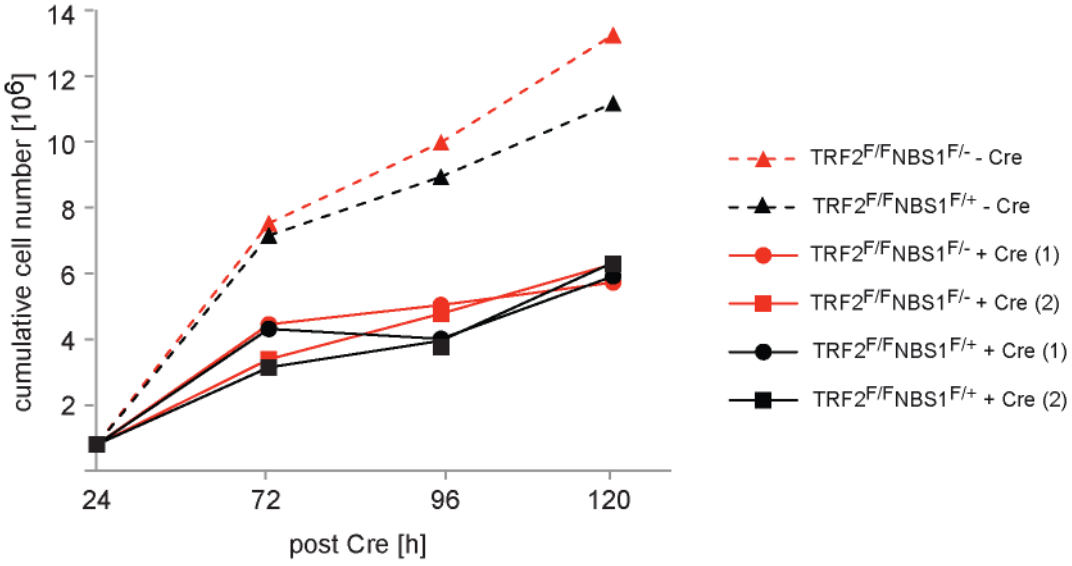

Supplemental figure 3 Dimitrova and de Lange

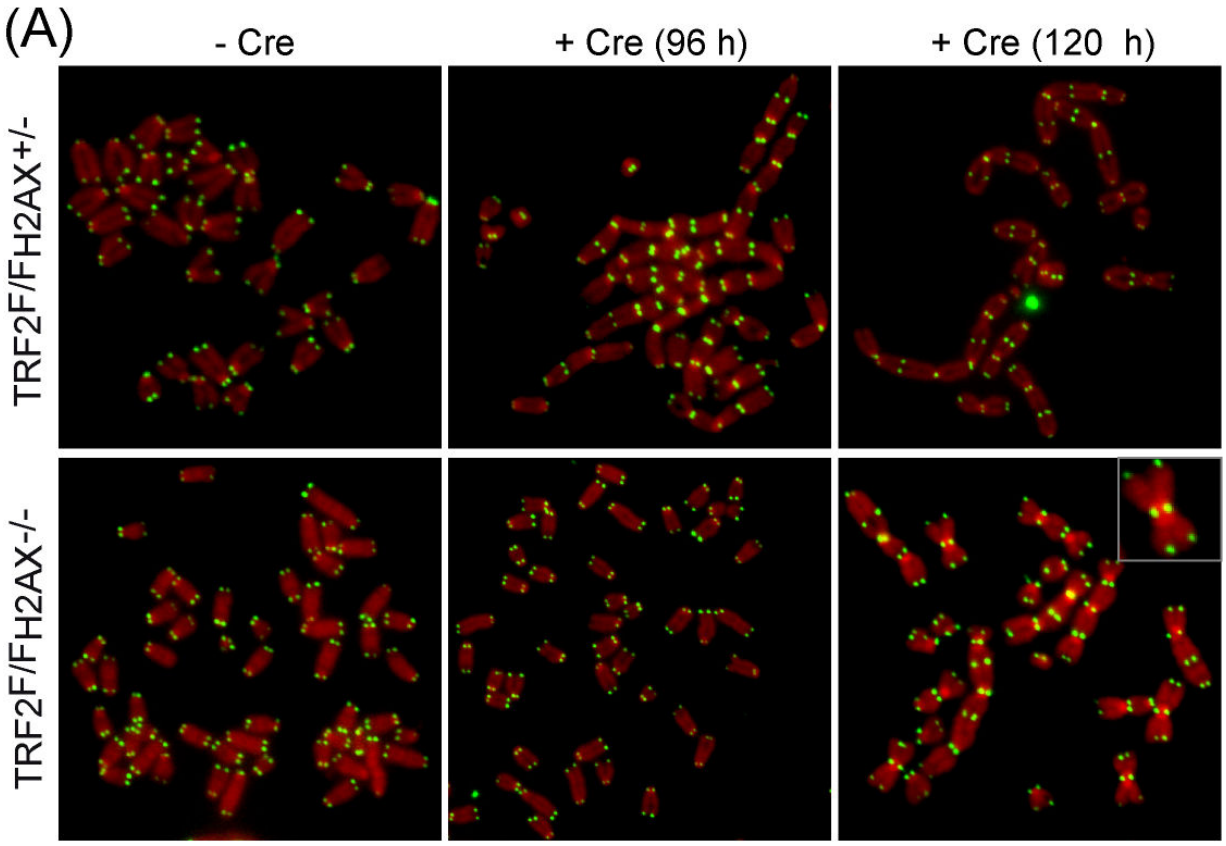

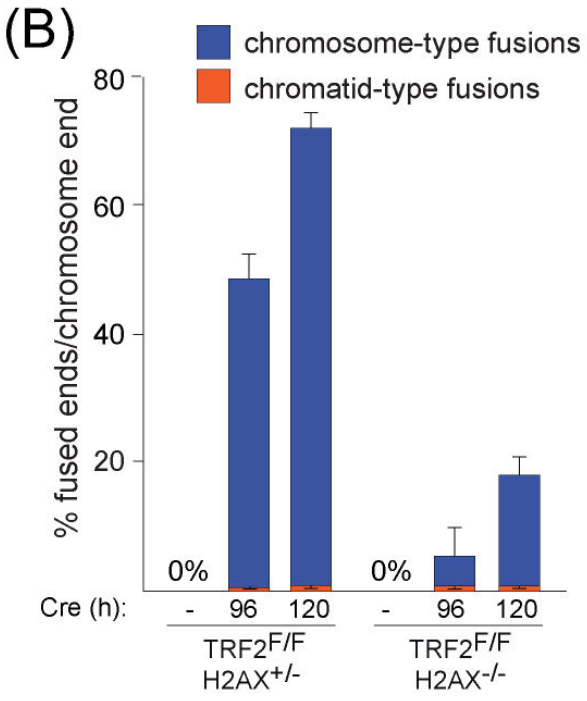

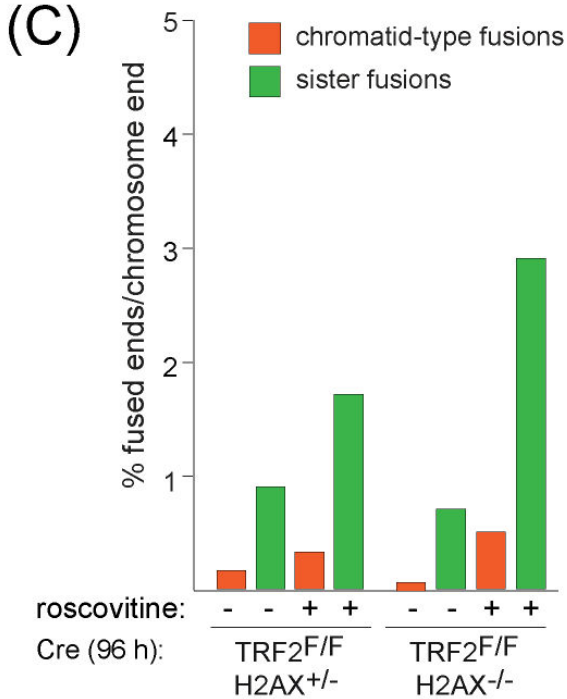

Supplementary Figure 4 Dimitrova and de Lange

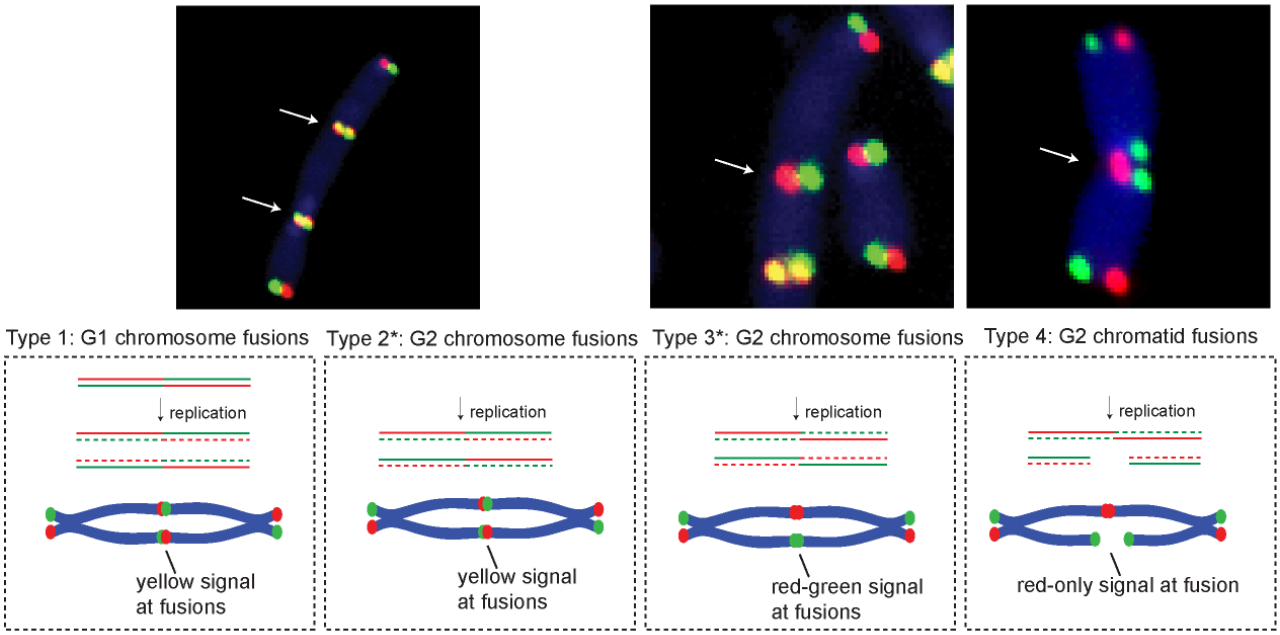

% fused ends/chromosome end

Cre (120 h)	Type 1 and 2	Type 3	Type 4
$TRF2^{F/F}NBS1^{F/+}$	74.3%	3%	0%
$TRF2^{F/F}NBS1^{F/-}$	4.2%	2.1%	7.6%